nature cell biology

Transient PLK4 overexpression accelerates tumorigenesis in p53-deficient epidermis

Özdemirhan Serçin[1], Jean-Christophe Larsimont[1], Andrea E. Karambelas[1], Veronique Marthiens[2], Virginie Moers[1], Bram Boeckx[3,4], Marie Le Mercier[5], Diether Lambrechts[3,4], Renata Basto[2] and Cédric Blanpain[1,6]

Aneuploidy is found in most solid tumours, but it remains unclear whether it is the cause or the consequence of tumorigenesis. Using *Plk4* overexpression (PLK4OE) during epidermal development, we assess the impact of centrosome amplification and aneuploidy on skin development and tumorigenesis. PLK4OE in the developing epidermis induced centrosome amplification and multipolar divisions, leading to p53 stabilization and apoptosis of epidermal progenitors. The resulting delayed epidermal stratification led to skin barrier defects. Plk4 transgene expression was shut down postnatally in the surviving mice and PLK4OE mice never developed skin tumours. Concomitant PLK4OE and *p53* deletion (PLK4OE/p53cKO) rescued the differentiation defects, but did not prevent the apoptosis of PLK4OE cells. Remarkably, the short-term presence of cells with supernumerary centrosomes in PLK4OE/p53cKO mice was sufficient to generate aneuploidy in the adult epidermis and triggered spontaneous skin cancers with complete penetrance. These results reveal that aneuploidy induced by transient centrosome amplification can accelerate tumorigenesis in p53-deficient cells.

Centrosomes are the microtubule-organizing centres of animal cells and participate in a variety of cellular processes such as cell division, and the establishment and maintenance of cell polarity[1,2]. Centrosome number is tightly regulated by several key centrosome duplication factors[3]. Abnormal centrosome number is associated with a variety of human diseases including cancer[4].

Since the pioneering observations of Boveri and Hansemann, centrosome amplification, defined by the presence of more than two centrosomes in a cell, has been associated with multipolar spindle assembly and consequent abnormal cell division[5]. Centrosome amplification has been reported during the early stage of tumorigenesis in different types of preneoplastic lesion such *in situ* breast ductal carcinomas[6] and *in situ* carcinomas of the uterine cervix, prostate, and female breast[7] suggesting that centrosome amplification could promote the early stage of tumorigenesis. Although complete inactivation of spindle assembly checkpoint components in mice is usually embryonic lethal, some hypomorphic alleles of these regulators lead to aneuploidy and, in some cases, are associated with an increase of tumour incidence, but often with incomplete penetrance and very late appearance[8–13]. However, several other mouse models leading to aneuploidy do not present increased tumour formation or even presented a decrease in tumour incidence[8,9,14–17], suggesting that either only some types of aneuploidy promote tumorigenesis or aneuploidy promotes tumour formation only in a specific cellular context.

Centrosome amplification is a hallmark of human tumours[18], but its contribution to tumorigenesis still remains an open question[8]. In flies, manipulation of the centrosome duplication machinery by overexpression of the master regulator of centriole biogenesis Plk4, also known as Sak, is a tumour-initiating event in transplantation assays[19]. Interestingly, the aetiology of these tumours seems to be different according to the tissue that contains extra centrosomes. Centrosome amplification in developing fly neuronal progenitors results in spindle positioning defects that lead to the expansion of the progenitor pool at the expense of differentiating cells[19]. However, these cells undergo bipolar division and maintain a highly stable diploid genome owing to the presence of highly efficient centrosome clustering mechanisms. In contrast, these clustering mechanisms were not efficient in fly epithelial cells with extra centrosomes, leading to the assembly and persistence of multipolar spindles that generated aneuploidy[20].

In mammals, the consequences of centrosome amplification have been evaluated only in the developing brain[21]. Overexpression of Plk4 in embryonic neural progenitors resulted in abnormal mitotic divisions generating aneuploidy and apoptosis leading to microcephaly. Aneuploid cells in the developing brain are rapidly removed from the cycling population by p53-dependent apoptosis[21].

[1]Université Libre de Bruxelles, IRIBHM, Brussels B-1070, Belgium. [2]Institut Curie, Centre de Recherche, Paris F-75248, France. [3]Laboratory for Translational Genetics, Department of Oncology, KU Leuven 3000, Belgium. [4]Vesalius Research Center, VIB, 3000 Leuven, Belgium. [5]Department of Pathology, Erasme Hospital, Université Libre de Bruxelles, Brussels B-1070, Belgium.
[6]Correspondence should be addressed to C.B. (e-mail: Cedric.Blanpain@ulb.ac.be)

Received 22 June 2015; accepted 19 October 2015; published online 23 November 2015; corrected online 10 December 2015; DOI: 10.1038/ncb3270

The deletion of *p53* in neural progenitors inhibits apoptosis of cells with extra centrosomes and aneuploidy but these cells did not give rise to brain tumours, leaving the question open of whether centrosome amplification and consequent aneuploidy can trigger tumorigenesis in mammals and if so in which context.

Non-melanoma skin cancers, basal cell carcinoma and squamous cell carcinoma represent the most frequent tumours in humans[22]. Squamous skin carcinoma (SCC) is the second most frequent skin cancer and contains mutations in Ras, p53 and other oncogenes or tumour-suppressor genes but also presented recurrent gene amplification and deletion of key driver genes[23]. Mouse models of skin SCCs recapitulate well the features of human skin SCCs. In mouse skin SCCs all tumour cells present some degree of aneuploidy[24]. In human SCCs, high levels of aneuploidy are associated with poorer prognosis[25], suggesting that skin SCC would represent an excellent model to study the role of aneuploidy in tumour initiation and progression.

Here, we used a genetic mouse model to assess the impact of PLK4OE and centrosome amplification in the formation of skin cancers. We overexpressed PLK4 in the developing skin epidermis and found that PLK4OE-mediated centrosome amplification led to abnormal mitosis and aneuploidy. The cells with centrosome supernumerary induced by PLK4OE were eliminated by apoptosis leading to a delay in skin stratification. However, simultaneous PLK4OE and p53 depletion in the epidermis allowed the survival of cells with extra centrosomes for a short period of time. Surprisingly, this transient presence of cells containing supernumerary centrosomes was sufficient to allow the accumulation of aneuploid cells in adult mice that invariably result in the formation of SCCs in 100% of the mice. Our data demonstrate that centrosome amplification followed by aneuploidy can accelerate tumorigenesis in mammals in the absence of p53.

RESULTS

PLK4 overexpression during embryonic development impairs skin stratification

To induce centrosome amplification in the skin epidermis, we crossed transgenic mice conditionally overexpressing PLK4 fused to the red fluorescent protein mCherry (mCherry–PLK4), which was previously used to induce centrosome amplification during brain development[21] with K14CRE (Supplementary Fig. 1). K14CRE mediated recombination in the mouse skin epidermis as early as embryonic day 12 (E12)[26], allowing the overexpression of mCherry–PLK4 during mouse skin epidermis development (Fig. 1a). In the skin epidermis, stem cells and progenitors are located within the basal compartment, whereas suprabasal cells contain terminally differentiated cells that do not proliferate any more[27]. Immunofluorescence analysis of skin epidermis at E14 showed that mCherry–Plk4 was expressed in the basal cells in K14CRE/mCherry–PLK4 mice (referred to as PLK4OE) and not in PLK4 single transgenic mice (Fig. 1a), demonstrating the initial recombination of the PLK4 transgene by K14CRE and the absence of leakiness in the absence of CRE expression. Co-immunostaining with the centrosome marker γ-tubulin showed that mCherry–PLK4 localized to centrosomes in the developing skin epidermis as previously reported during mouse brain development[21] (Supplementary Fig. 2a) and following PLK4OE *in vitro*[28,29] and 90% of the cells expressing mCherry–PLK4 exhibited centrosome amplification (Supplementary Fig. 2b), demonstrating the efficient induction of centrosome amplification in the developing skin epidermis in response to PLK4 overexpression.

PLK4OE mice were born alive at Mendelian ratios and showed shiny skin and an open eyelid phenotype in the most affected mice (Supplementary Fig. 3). However, about 50% of PLK4OE mice died within 24 hours after birth (Fig. 1b). The shiny appearance of the neonatal skin is usually associated with skin barrier defects that can lead to rapid dehydration and neonatal lethality[30]. To assess whether PLK4OE induced defects in skin barrier formation, we performed a toluidine dye penetration assay at E17.5, a time point at which wild-type epidermis had already acquired a functional skin barrier[31] (Fig. 1c). Two-thirds of PLK4OE mice at E17.5 presented severe skin barrier defects, as shown by the almost complete penetration of the toluidine dye in the ventral and dorsal skin, which was never observed in control wild-type littermates at this stage of development (Fig. 1c). These data indicate that PLK4 overexpression in the developing skin epidermis causes defects in skin barrier formation and neonatal lethality.

To determine the cause of the skin barrier defects observed in PLK4OE mice, we assessed the histology and expression of epidermal differentiation markers at different time points during embryonic and postnatal development (Fig. 1d–i). We found that at E16.5 and postnatal day 1 (P1) in PLK4OE mice, which present shiny skin, PLK4OE epidermis was thinner and presented fewer layers of suprabasal spinous cells expressing K1 and K10 (Fig. 1d–f,h) and a decreased number of granular layers expressing loricrin compared with control littermates (Fig. 1g). However, the surviving PLK4OE mice at P7 presented normal epidermis, without defects in skin differentiation (Fig. 1d–i). These data show that PLK4 overexpression in the skin epidermis induces a developmental delay of skin stratification.

PLK4 overexpression induced epidermal progenitor apoptosis

To understand why PLK4OE mice that survived the postnatal lethality present normal skin epidermis at later time points, we assessed mCherry–PLK4 transgene expression over time (Fig. 2a–c). We found that between E16.5 and P1, about 30% of the basal epidermal cells expressed mCherry–PLK4 protein irrespective of their mitotic activity whereas at postnatal P7 and thereafter, mCherry–PLK4-expressing cells were no longer detected in PLK4OE epidermis (Fig. 2a,b). To identify the reason for the progressive loss of PLK4OE cells over time, we assessed the degree of transgene recombination and mCherry–*PLK4* messenger RNA (mRNA) expression over time. Quantitative PCR (qPCR) analysis showed that more than 95% of the genomic DNA *Plk4* transgene of basal epidermal cells was recombined at E16.5, and basal cells were not replaced by cells that that did not recombine the *PLK4* transgene over time (Fig. 2d). In contrast, qPCR with reverse transcription (qRT–PCR) analysis showed that mCherry–PLK4 mRNA expression in the same cells was readily detectable at E17 and P1, but no longer detectable in adult mice (Fig. 2c), in agreement with the immunostaining results of mCherry–PLK4 in skin sections (Fig. 2a), and consistent with the complete transcriptional shut down of the mCherry–PLK4 transgene during postnatal development. These data demonstrate that a strong selective pressure occurred during development and early postnatal life to eliminate cells expressing mCherry–PLK4 in the skin epidermis.

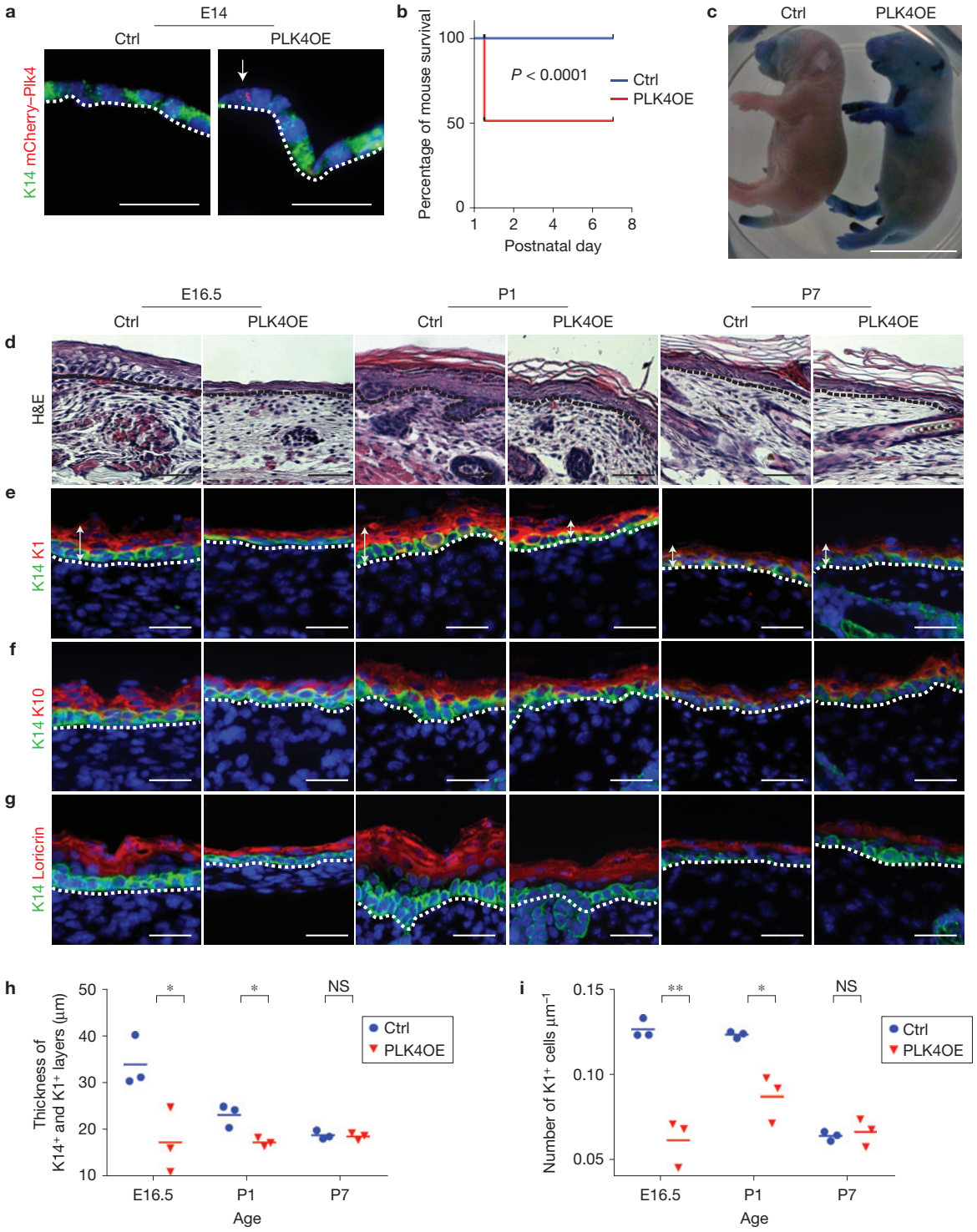

Figure 1 PLK4 overexpression impairs skin stratification. (**a**) Immunofluorescence of skin sections at E14 showing the expression of the *mCherry–Plk4* transgene in basal K14$^+$ keratinocytes in control and PLK4OE mice. Arrow shows a basal cell overexpressing mCherry–Plk4. (**b**) Mouse survival curve of the PLK4OE mice ($n=30$ mice for each genotype at P1, $n=57$ or 32 mice at P7 control and PLK4OE respectively, $P<0.0001$, Mantel–Cox). (**c**) Toluidine blue skin penetration assay performed at E17.5. Four out of the six PLK4OE mice and 0 out of 6 control littermates show dye penetration in the ventral and dorsal skin. (**d**–**g**) Skin sections from E16.5, P1 and P7 control and PLK4OE mice were stained with haematoxylin and eosin (**d**) or immunostained for K14 (**e**–**g**) and the differentiation markers K1 (**e**), K10 (**f**) and loricrin (**g**). Black or white dotted lines represent the basal lamina. (**h**) Quantification of the thickness of the basal and spinous layers (K14$^+$ and K1$^+$), as shown by arrows in **e** in control and PLK4OE mice. Skin thickness was measured as shown by arrows in **e** ($\geq$27 regions counted per mouse and time point). Data represent the mean of $n=3$ mice. (**i**) Quantification of the number of spinous cells (K1$^+$ cells) per length of the tissue in control and PLK4OE mice ($\geq$300 cells counted per mouse and time point). Data represent the mean of $n=3$ mice. ($^*P<0.05$, $^{**}P<0.005$ and NS (not significant) indicates $P>0.05$; two-tailed Student *t*-test). Nuclei were stained with DAPI. Scale bars, 50 μm (**a**,**d**–**g**) and 1 cm (**c**). Source data are available in Supplementary Table 1.

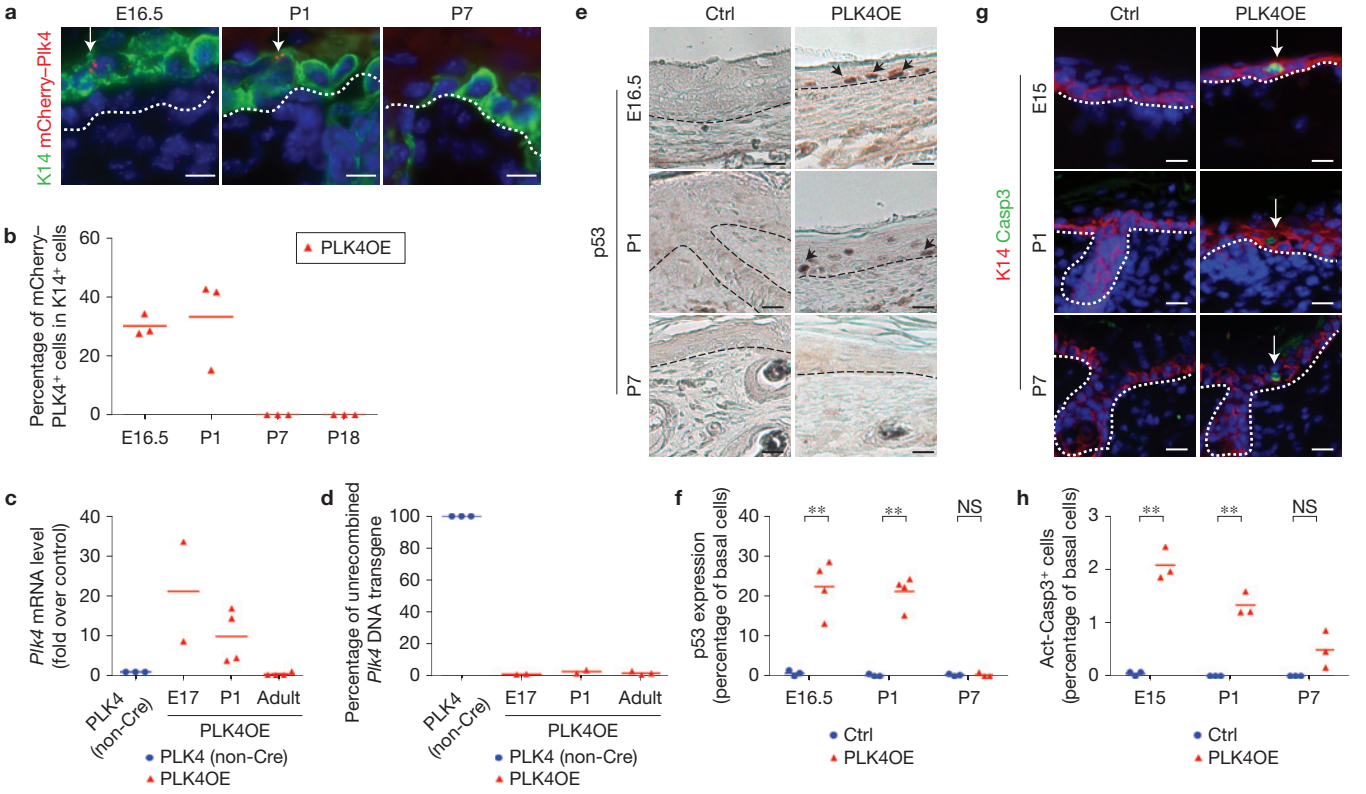

Figure 2 PLK4 overexpression induced epidermal progenitor apoptosis. (**a**) Immunofluorescence analysis of mCherry–PLK4 and K14 in PLK4OE epidermis showing the progressive decrease of mCherry–PLK4-positive cells over time. Arrows mark a basal keratinocyte overexpressing mCherry–Plk4. (**b**) Quantification of mCherry–PLK4 expression in K14$^+$ keratinocytes. ≥270 cells counted per PLK4OE ($n=3$ mice for each time point). No statistical test was performed. (**c**) RT–qPCR expression analysis of mCherry–PLK4 mRNA in control and PLK4OE epidermis. Fold changes were calculated using the ΔΔCT method after normalization over β-actin. Data show the mean of $n=2$ (E17), 4 (P1) or 4 (non-Cre and adult), respectively. (**d**) qPCR analysis of the unrecombined PLK4 transgene in basal epidermal cells isolated from E16.5, P1 and adult PLK4OE mice and control mice with no *CRE*. Fold changes were calculated using the ΔΔCT method after normalization over β-actin. Data show the mean of $n=2$ (E17, P1) or 3 mice (non-Cre and adult), respectively. (**e**) Immunohistochemistry for p53 in control and PLK4OE skin sections. Arrows mark cells expressing p53. (**f**) Quantification of p53-positive cells in basal cells over time (≥250 basal cells counted per mouse and time point; $n=3$ control mice (for all time points) and $n=4$ mice (E16.5 and P1) and $n=3$ (P7) PLK4OE). (**g**) Immunofluorescence for active caspase-3 and K14 in skin sections of control and PLK4OE mice. Arrows show caspase-positive cells. (**h**) Quantification of active caspase-3-positive cells in control and PLK4OE epidermis at E15, P1 and P7 (≥1,000 basal cells counted per mouse and time point). Data represent the mean of $n=3$ mice of control or PLK4OE mice ($^{**}P<0.005$ and NS indicates $P>0.05$. Two-tailed Student's *t*-test). Nuclei were stained with DAPI and scale bars represent 10 μm. Source data are available in Supplementary Table 1.

We then assessed whether the loss of mCherry–PLK4-positive cells and the delay in stratification was due to p53-dependent apoptosis, as shown in the developing brain[21] and in human retinal pigment epithelial cells *in vitro*[29]. Immunohistochemistry of p53 showed that about 25% of basal PLK4OE keratinocytes were positive for p53 from E16.5 to P1, whereas p53-positive cells were not observed in control littermates at any stage of epidermis development (Fig. 2e,f). However, at P7, p53-positive cells were no longer found in the epidermis of PLK4OE mice (Fig. 2e,f). To determine whether p53 stabilization was associated with apoptosis[32], we assessed the expression of active caspase 3 during embryonic and early postnatal development. At E15, more than 2% of basal epidermal cells in PLK4OE mice were positive for active caspase 3, which is similar to the proportion of apoptotic cells observed following exposure to 20 Gy ionizing radiation[33], indicating that PLK4OE induced apoptosis of epidermal cells (Fig. 2g,h). The proportion of apoptotic cells in PLK4OE epidermis progressively decreased over time postnatally and apoptotic cells were no longer detected at P7 (Fig. 2g,h). These results show that PLK4OE cells are eliminated by apoptosis during embryonic and early postnatal development and are replaced postnatally by epidermal cells in which the mCherry–PLK4 transgene was epigenetically/transcriptionally shut down, supporting the notion that a strong selective pressure acts to eliminate PLK4OE cells.

PLK4 overexpression induced p53-dependent and -independent apoptosis

To determine whether the disappearance of PLK4OE cells over time is mediated by p53-dependent apoptosis as has been proposed during mouse brain development[21], we induced PLK4OE in p53-deficient epidermis. To this end, we generated triple transgenic *K14CRE/PLK4–mCherry/p53$^{f/f}$* mice (PLK4OE/p53cKO) to determine whether p53 deletion rescues the developmental delay and apoptosis observed in PLK4-overexpressing epidermal cells. Neonatal lethality of PLK4OE mice was completely rescued by concomitant *p53* deletion in the epidermis (30 out of 30 mice). The absence of neonatal lethality in PLK4OE/p53cKO mice was the consequence of the restoration of skin

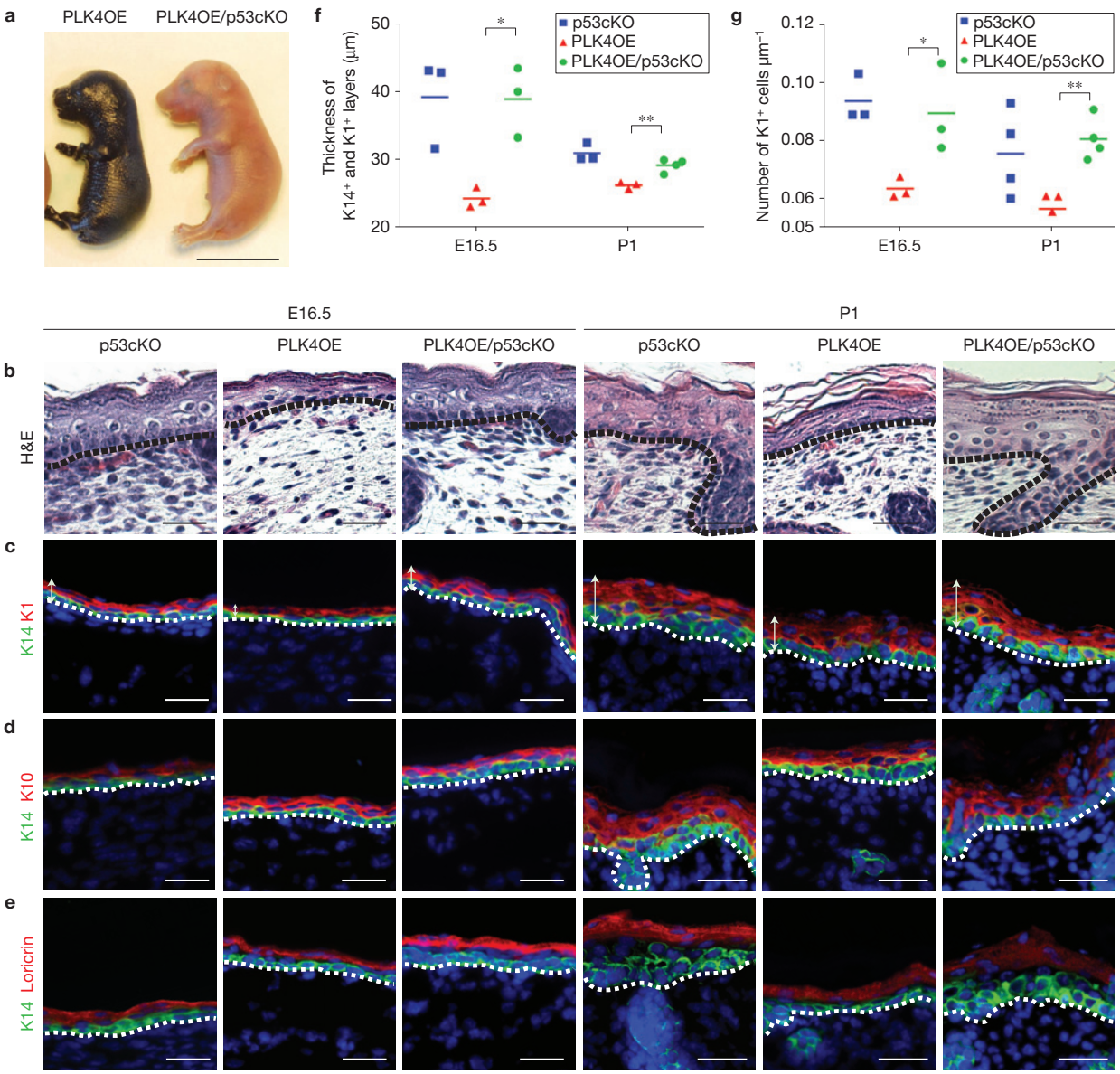

Figure 3 p53 deletion rescues the defect of skin stratification in PLK4OE mice. (**a**) Toluidine blue dye penetration assay performed at E17.5 in PLK4OE and PLK4OE/p53cKO. Five out of the six PLK4OE/p53cKO and six out of the six control littermates show normal skin barrier formation at E17.5 (scale bar, 1 cm). (**b**–**e**) Expression of epidermal differentiation markers in p53cKO, PLK4OE and PLK4OE/p53cKO mice. Skin sections were stained with haematoxylin and eosin (**b**) or immunostained for K14 (**c**–**e**), K1 (**c**), K10 (**d**) and loricrin (**e**). Dotted lines represent the basal lamina. Scale bars, 50 µm. (**f**) Quantification of the thickness of the basal and spinous layers ($K14^+$ and $K1^+$) in PLK4OE, PLK4OE/p53cKO and p53cKO mice. Skin thickness was measured on immunofluorescence pictures using the ZEISS/AxioVision LE as shown in **c** (≥27 regions counted per mouse and time point, data represent the mean of $n=3$ mice for E16.5 and P1 (p53cKO or PLK4OE), $n=3$ mice for E16.5 PLK4OE/p53cKO, and $n=4$ mice for P1 PLK4OE/p53cKO). (**g**) Quantification of number of spinous cells ($K1^+$ cells) per length of the tissue in PLK4OE, PLK4OE/p53cKO and p53cKO mice (≥300 cells counted per mouse and time point). Data represent the mean of $n=3$ mice for E16.5 p53cKO, PLK4OE or PLK4OE/p53cKO and $n=4$ mice for P1 p53cKO or PLK4OE/p53cKO or 3 mice for P1 PLK4OE ($^*P<0.05$, $^{**}P<0.005$ and NS indicates $P>0.05$. Two-tailed Student *t*-test). Source data are available in Supplementary Table 1.

barrier function as shown by the absence of toluidine dye penetration at E17.5 (Fig. 3a), demonstrating that p53 deficiency rescues the lethality associated with skin barrier defects in PLK4OE mice.

To determine the mechanisms by which p53 deletion rescues skin barrier defects in PLK4OE epidermis, we assessed the histology and expression of differentiation markers during embryonic and postnatal skin development in PLK4OE/p53cKO mice (Fig. 3b–g). In contrast to PLK4OE mice that present defects in epidermal differentiation, PLK4OE/p53cKO epidermis showed similar numbers of layers of basal and suprabasal differentiated cells as control littermates at E16.5 and P1 (Fig. 3b–g). These data show that *p53* deletion rescues skin differentiation defects mediated by PLK4OE in the epidermis.

We then assessed whether the rescue of epidermal differentiation mediated by p53 deletion was due to a decrease in apoptosis in

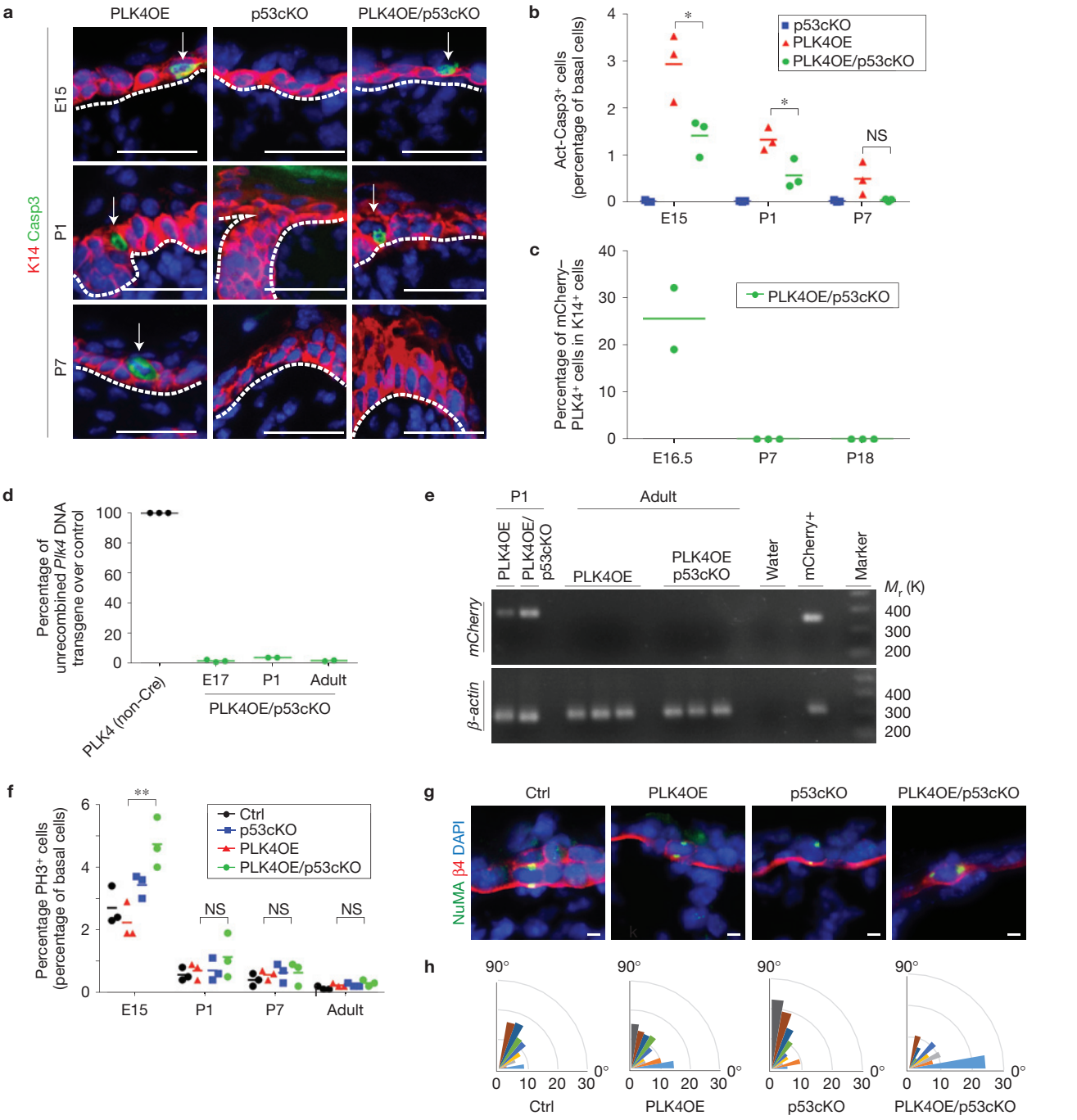

Figure 4 PLK4 overexpression induced p53-dependent and -independent apoptosis. (**a**) Immunofluorescence for active caspase 3 and K14 in skin sections. Only PLK4OE and PLK4OE/p53cKO mice (but not p53cKO) show apoptosis (arrows). Dotted lines mark the basal lamina. Dotted lines mark the basal lamina. Scale bars, 50 μm. (**b**) Quantification of active caspase-3-positive cells in **a**. ≥1,000 basal cells counted per mouse and time point data represent the mean of $n=3$ mice for p53cKO, PLK4OE or PLK4OE/p53cKO. (**c**) Quantification of mCherry–PLK4 expression in $K14^+$ keratinocytes over time (≥270 cells counted per mouse and time point, data represent the mean of $n=2$ (E16.5) and 3 mice for (P7 and P18). (**d**) qPCR analysis of the unrecombined DNA PLK4 transgene in E17, P1 and adult mice over control (PLK4 non-Cre). Data represent the mean of $n=3$ mice (E17) for each genotype and 2 mice (P1 and adult). Fold changes were calculated using the ΔΔCT method after normalization over β-actin. PLK4 non-Cre mice were considered as 100% unrecombined. (**e**) RT–PCR expression analysis of mCherry–PLK4 and β-actin (control) mRNA in P1 and adult PLK4OE and PLK4OE/p53cKO skin. An unprocessed original scan of the gel is shown in Supplementary Fig. 5. (**f**) Quantification of basal cell ($K14^+$) proliferation using immunofluorescence of K14 and PH3 in skin sections (≥641 basal cells counted per mouse and per time point); data represent the mean and individual values from $n=3$ mice for each time point (E15, P1, P7 and adult) and genotype (control, p53cKO, PLK4OE and PLK4OE/p53cKO). (**g**) Immunofluorescence for NuMA and β_4-integrin was performed on E15.5 embryos to determine the angle of division with respect to the basal lamina. (**h**) Quantification of the angle between the spindle pole and basal lamina as shown in **g**. Every bar represents the mean angle of 10 cells (≥198 $NuMA^+$ basal cells counted per genotype). Data represent angle values from $n=2$ p53cKO, 6 control, 5 PLK4OE and 3 PLK4OE/p53cKO mice (no statistical test was performed for **g**). $^*P<0.05$, $^{**}P<0.005$ and NS indicates $P>0.05$; two-tailed Student *t*-test. Source data are available in Supplementary Table 1.

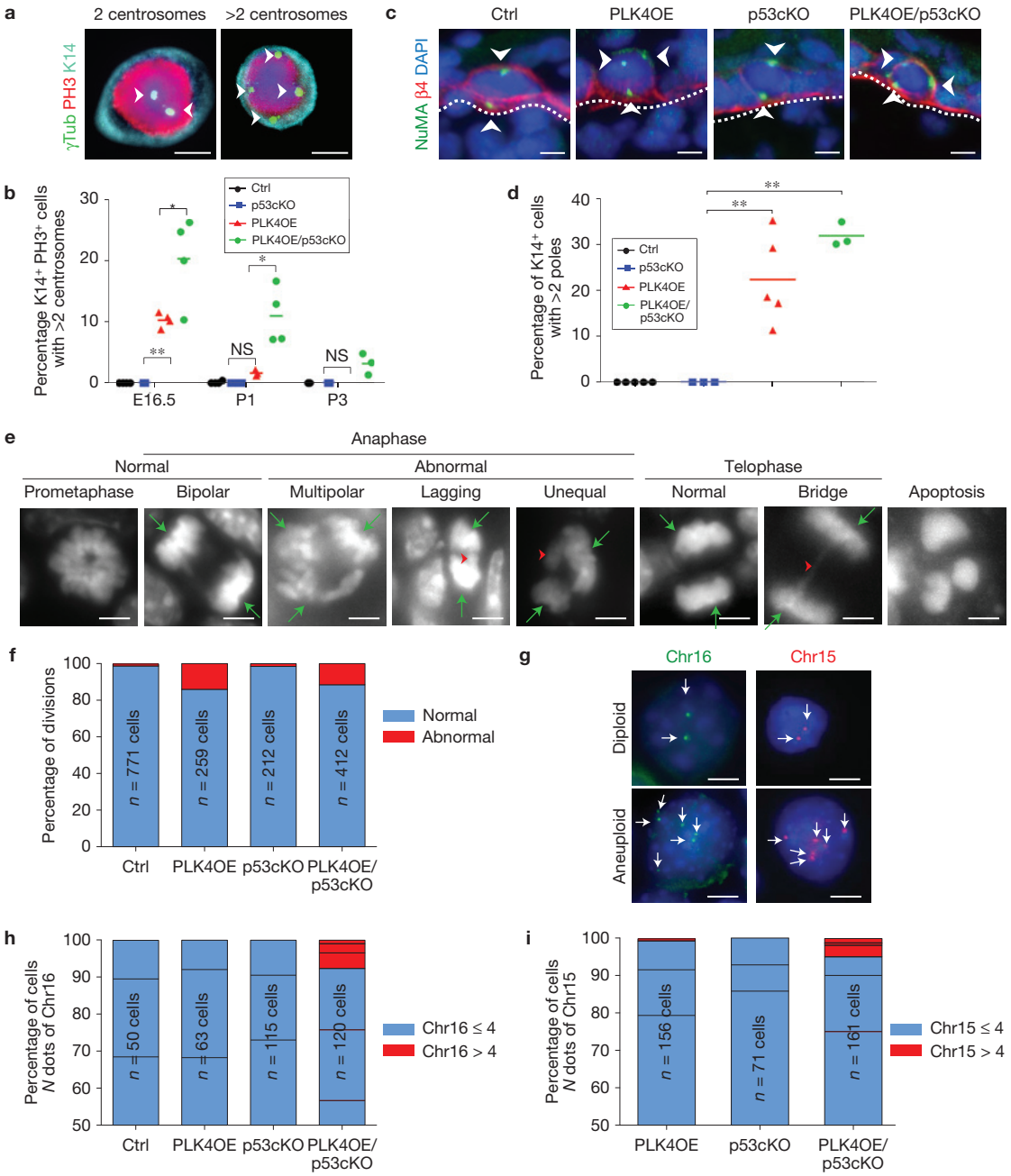

Figure 5 PLK4 overexpression causes aneuploidy only in p53-deficient progenitors. (**a**) Immunofluorescence for K14, the centrosomal marker γ-tubulin and the mitotic marker phospho-histone 3 (PH3) to detect mitotic basal cells with more than 2 centrosomes on cytospin. Arrows mark the centrosomes. (**b**) Quantification of basal mitotic $K14^+PH3^+$ cells with >2 centrosomes (γ-tubulin) in control, PLK4OE, p53cKO and PLK4OE/p53cKO epidermis (≥50 cytospun mitotic basal cells were counted for each mouse). Data represent the mean value at E16.5 of $n=4$ control, PLK4OE and PLK4OE/p53cKO mice, and $n=3$ p53cKO mice; at P1, $n=4$ control, p53cKO and PLK4OE/p53cKO mice, and $n=3$ PLK4OE mice; and at P3 $n=3$ control, p53cKO and PLK4OE/p53cKO mice. (**c**) Immunofluorescence for NuMA and β_4-integrin was performed on E15.5 embryos sections to visualize multipolar divisions in control, PLK4OE, p53cKO and PLK4OE/p53cKO mice. Dotted lines mark the basal lamina and arrows mark the centrosomes. (**d**) Quantification of basal mitotic cells with >2 spindle poles as shown by NuMA immunofluorescence in **c**; a total of ≥198 $NuMA^+$ basal cells counted per genotype; data represent mean values from $n=6$, 3, 5 and 3 mice from control, p53cKO, PLK4OE and PLK4OE/p53cKO respectively. (**e**,**f**) Immunofluorescence analysis (**e**) and quantification (**f**) of normal and abnormal mitotic figures (multipolar, unequal, lagging and bridge) observed by Hoechst nuclear staining in PLK4OE and PLK4OE/p53cKO keratinocytes. Data represent the mean from $n=4$, 3, 2 or 3 mice and a total of 771, 259, 212 or 412 cells from each genotype for control, PLK4OE, p53cKO and PLK4OE/p53cKO, respectively. No statistical test was performed. (**g**–**i**) FISH using probes against chromosome 16 (green) and 15 (red) performed on cytospin of epidermal cells isolated at E16.5 from PLK4OE, p53cKO and PLK4OE/p53cKO mice. Arrows show dots for Chr15 or Chr16. (**h**,**i**) Quantification of the percentage of cells with more than 4 chromosome dots per cell in the different mouse genotypes for Chr16 (**h**) and Chr15 (**i**). (50, 63, 115 or 120 cells in **h** and 0, 156, 71, 161 cells in (**i**) counted per $n=1$ mouse control from PLK4OE, p53cKO, PLK4OE/p53cKO; respectively; no statistical test was performed). $^*P<0.05$, $^{**}P<0.005$ and NS indicates $P>0.05$; two-tailed Student *t*-test. Source data are available in Supplementary Table 1. Nuclei were stained with DAPI and scale bars represent 5 μm.

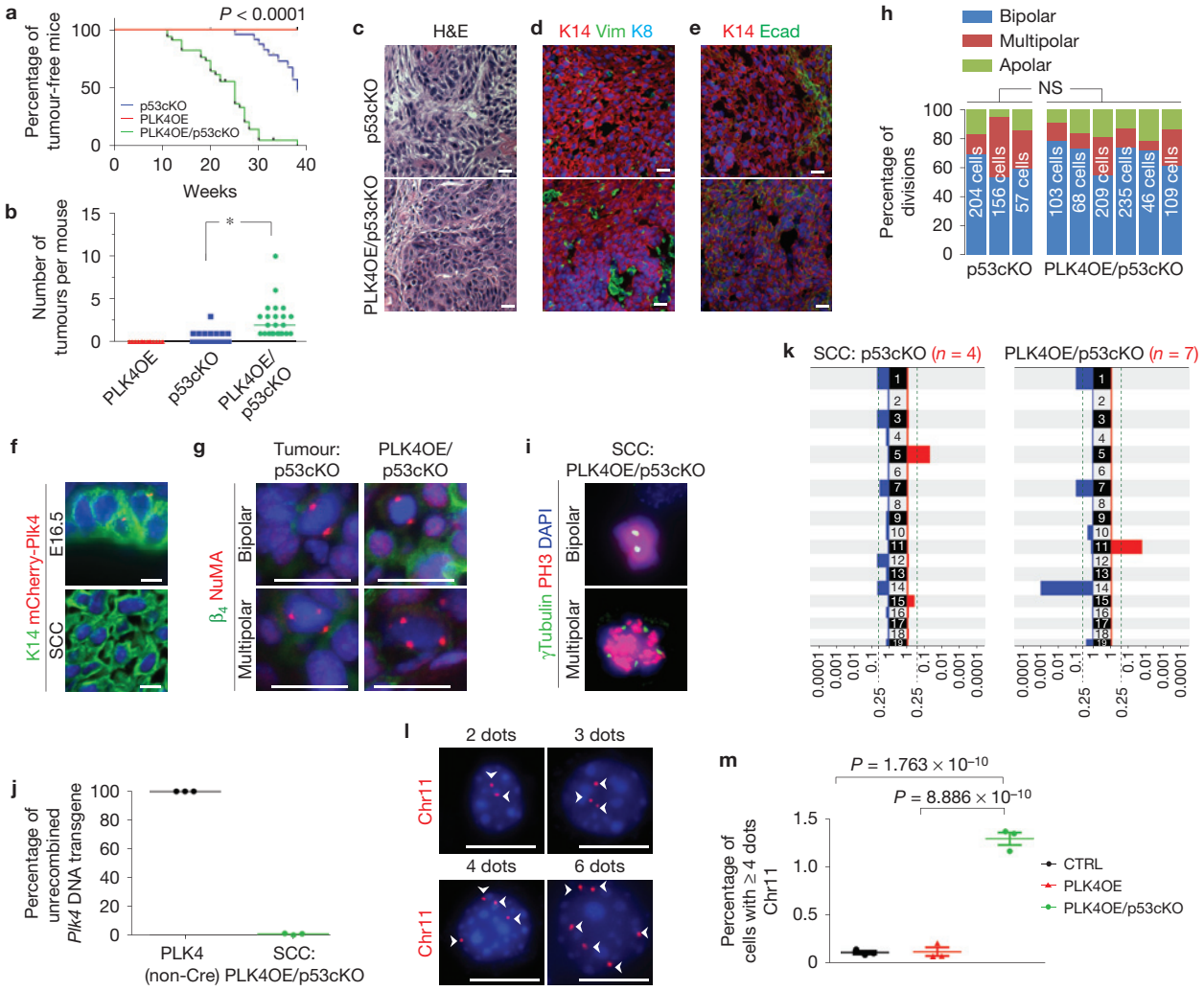

Figure 6 PLK4OE in p53-deficient progenitors accelerates skin tumour formation. (**a**) Skin-tumour-free survival as quantified by the presence of macroscopic skin tumours ($P < 0.0001$, Mantel–Cox). Data represent survival of $n = 14$, 26 or 32 PLK4OE, p53cKO or PLK4OE/p53cKO mice over 40 weeks. None of the control or PLK4OE mice developed skin tumours 40 weeks after birth. (**b**) Number of skin tumours in $n = 14$, 23 or 23 PLK4OE, p53cKO or PLK4OE/p53cKO mice, respectively. $^*P < 0.05$, two-tailed Student's *t*-test. (**c**–**e**) Representative histology of well-differentiated SCCs arising from PLK4/p53cKO and p53cKO stained with H&E (**c**), K14, K8 and vimentin (**d**) and K14 and Ecad (**e**). (**f**) Immunofluorescence for PLK4–mCherry in sections of PLK4OE embryos at E16.5 and in PLK4OE/p53cKO tumours. (**g**,**h**) Tumours from p53cKO or PLK4OE/p53cKO were stained with NuMA and β_4-integrin. (**h**) Quantification of individual tumours classified as apolar, multipolar and bipolar from **g**; 204, 156, 57 NuMA$^+$ cells in p53cKO tumours from $n = 3$ mice and 103, 68, 209, 235, 46, 109 NuMA$^+$ cells in PLK4OE/p53cKO tumours from $n = 5$ mice. (**i**) PLK4OE/p53cKO tumour cells stained with γ-tubulin and PH3. (**j**) qPCR analysis of the unrecombined PLK4 transgene in PLK4OE/p53cKO tumours over control (PLK4 no-cre) obtained from $n = 3$ mice in each group. Fold changes were calculated using the ΔΔCT method after normalization over β-actin. Control PLK4 non-Cre mice were considered 100% unrecombined. (**k**) GISTIC analysis of low-coverage whole-genome sequencing of SCCs arising from PLK4OE/p53cKO mice ($n = 7$) and p53cKO mice ($n = 4$) shows whole-chromosome deletion and amplification of specific chromosomes in PLK4OE/p53cKO tumours. Scale represents *Q* values. (**l**) FISH using probes against chromosome 11 performed on cytospin of epidermal cell isolated from adult epidermis of PLK4OE, p53cKO and PLK4OE/p53cKO mice. Arrowheads mark the dots for Chr11. (**m**) Quantification of the proportion of cells with four or more dots of Chr 11 in **l** per cell in $n = 3$ mice each genotype (≥1,000 cells counted per mouse). Fisher's exact test was used to assess statistical significance. Nuclei were stained with DAPI. Scale bars, 10 μm. Source data are available in Supplementary Table 1.

PLK4OE mice. Surprisingly and in sharp contrast to what was found in neuronal progenitors[21], *p53* deletion did not completely prevent apoptosis in PLK4OE epidermis, but led to a significant inhibition of basal progenitor apoptosis, which progressively decreased over time, to become undetectable at P7 (Fig. 4a,b). The p53-independent cell death observed here also led to a parallel reduction in the number of mCherry–PLK4-expressing cells in PLK4OE/p53cKO epidermis, as shown by immunostaining or RT–PCR analysis (Fig. 4c–e) despite the almost complete DNA recombination of the PLK4 transgene in PLK4OE/p53cKO mice (Fig. 4d), similarly to what we observed in PLK4OE mice (Fig. 2a–d). Interestingly, as shown by PH3 immunostaining, PLK4OE/p53cKO presented a slightly higher percentage of mitotic cells at E15 and P1 when compared with control and PLK4OE mice (Fig. 4f).

During embryonic development, mitotic spindle orientation and the proportion of symmetric versus asymmetric division in basal

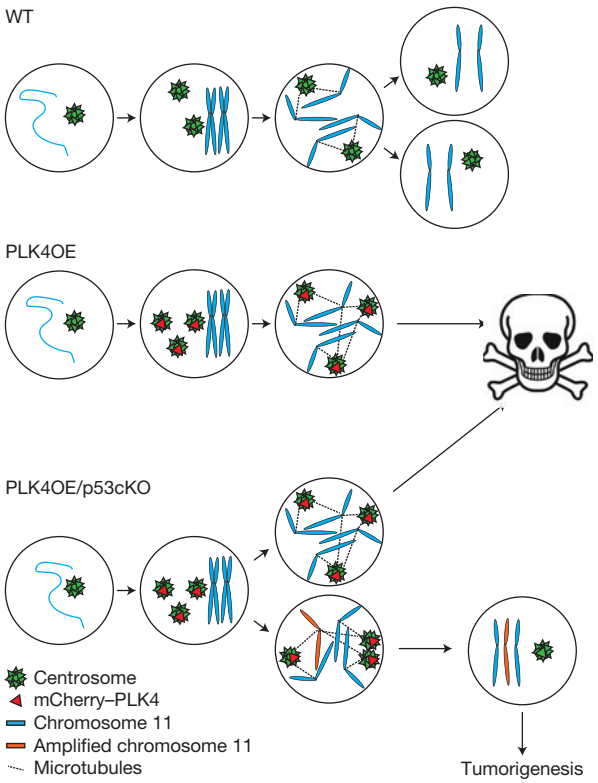

Figure 7 Model of skin tumorigenesis mediated by PLK4OE in p53-deficient epidermis. In wild-type epidermis, progenitors contain two centrosomes and divide in a bipolar manner, resulting in equal distribution of DNA between the two daughter cells. PLK4OE in epidermal progenitors induces centrosome supernumerary, inducing multipolar cell division, which is incompatible with cell survival. In contrast, PLK4OE in p53-deficient epidermis leads to survival of aneuploid cells (for example, amplification of chromosome 11), which persist in adult life, and induce tumour formation despite the absence of PLK4OE.

epidermal cells regulates the early stage of skin stratification[34,35]. By measuring the angle of the spindles with respect to the basal lamina, we assessed the impact of PLK4OE and *p53* deletion on the proportion of symmetric versus asymmetric divisions in the developing epidermis. Although at E15.5, most of the divisions in basal cells with 2 centrosomes of control and p53cKO mice were perpendicular to the basal lamina as previously described[34], we observed a strong increase in parallel divisions in PLK4OE/p53cKO mice (Fig. 4g,h), consistent with an increase in symmetric self-renewing divisions at this stage of development, suggesting that these cells are replenishing the basal cells that are dying by apoptosis. Together, our data show that PLK4OE stimulates p53-dependent and p53-independent mechanisms that trigger the activation of caspase 3 and apoptosis of cells with extra centrosomes. In addition, PLK4 is transcriptionally shut down irrespective of p53 expression. The higher percentage of mitotic cells and the increase in self-renewing divisions in the absence of p53 in PLK4OE cells may explain why p53 deletion rescues the defect of stratification and barrier formation.

PLK4 overexpression causes aneuploidy only in p53-deficient progenitors

To determine the fate of progenitor cells undergoing abnormal mitosis, we assessed the prevalence of centrosome amplification in embryonic and newborn mice following PLK4OE in wild-type and *p53*-deficient background (Fig. 5a,b). At E16.5, 10% and 20% of dividing (Ser28-phospho-histone H3-positive) PLK4OE and PLK4OE/p53cKO basal cells contain extra centrosomes (Fig. 5a,b). By analysing NuMA expression in PLK4OE and PLK4OE/p53KO mice, which is localized at the spindle pole/centrosome during mitosis[36], we found a similar percentage of multipolar cells at E15.5 (Fig. 5c,d). By P1, a very large fraction of the dividing epidermal progenitor cells in PLK4OE/p53cKO mice contained extra centrosomes (10% of the dividing basal progenitors), whereas PLK4OE basal progenitors did not contain any cells with more than 2 centrosomes at this point (Fig. 5b). At P3, cells with more than 2 centrosomes were not observed any more in PLK4OE epidermis in the presence or absence of p53 (Fig. 5b), demonstrating the strong selective pressure against cells with centrosome amplification in the skin epidermis, and suggesting the existence of a highly robust mechanism that eliminates all cells with extra centrosomes even in the absence of p53.

To determine whether centrosome amplification leads to chromosome segregation errors and consequent aneuploidy, we assessed DNA segregation during mitosis in WT and PLK4OE mice at E16.5. Although WT epidermal progenitors did not present any mitotic abnormalities, PLK4OE and PLK4OE/p53cKO epidermis presented similar frequencies of abnormal divisions (Fig. 5e,f). Signs of apoptosis seen by nuclear fragmentation were observed in both PLK4OE and PLK4OE/p53cKO mice (Fig. 5e). Consistent with increased abnormal divisions seen in PLK4OE/p53cKO mice, fluorescence *in situ* hybridization (FISH) using probes against mouse chromosomes 15 and 16 demonstrated that 6–8% of the basal cells of PLK4OE/p53cKO mice at E16.5 show more than 2 copies of either chromosome (Fig. 5g–i), whereas cells from control (no CRE), PLK4OE or p53cKO epidermis presented 2 to 4 dots for chromosomes 15 and 16 depending on the cell cycle stage (Fig. 5g–i), further demonstrating the generation of aneuploidy that occurs following transient accumulation of extra centrosomes during epidermal development.

PLK4OE in p53-deficient progenitors accelerates skin tumour formation

Control and PLK4OE mice never developed spontaneous skin tumours (Fig. 6a). In sharp contrast, all PLK4OE/p53cKO mice developed spontaneous tumours with complete penetrance with an average latency of 25 weeks (25 ± 8 weeks), whereas p53cKO mice developed skin tumours with a much longer latency (38 ± 11 weeks) and with incomplete penetrance at least until 40 weeks (only 50% of the p53cKO mice developed skin tumours by 4 weeks of age) as previously reported[37]. In addition, PLK4OE/p53cKO mice developed on average several tumours per mouse (mean: 2.56 ± 0.44) whereas p53cKO mice have only one or no tumours per mouse (mean: 0.4 ± 0.15; Fig. 6b). Immunohistological characterization showed that PLK4OE/p53cKO and p53cKO tumours were similar and consisted of well-differentiated invasive SCCs expressing K14 and E-cadherin and negative for K8 and vimentin, which is expressed by stromal cells (Fig. 6c–e). Immunostaining showed that mCherry–PLK4 was not expressed in PLK4OE/p53cKO tumours (Fig. 6f). Analysis of centrosome number using NuMA and γ-tubulin immunostaining showed that most tumour cells presented two centrosomes,

although multipolar divisions were occasionally observed in both PLK4OE/p53cKO and p53cKO SCCs (Fig. 6g–i), suggesting that centrosome numerical defects can arise in tumour cells independently of the presence of PLK4OE. Importantly, qPCR analysis showed that PLK4OE/p53cKO tumours presented the recombined *PLK4* transgene demonstrating that tumour-initiating cells had overexpressed PLK4 during tumorigenesis (Fig. 6j and Supplementary Fig. 4).

Low-coverage whole-genome sequencing showed that all PLK4OE/p53cKO SCCs were aneuploid containing gain and loss of whole chromosomes (Fig. 6k), whereas control bone marrow from the same animals showed diploid genome. Genomic Identification of Significant Targets in Cancer (GISTIC) analysis for recurrent whole-chromosome copy number alteration in PLK4OE/p53cKO SCCs identified statistically significant recurrent deletions of chromosomes 1, 7 and 14 and amplification of chromosome 11 (Fig. 6k).

To assess whether the specific chromosome alterations found in PLK4OE/p53cKO SCCs were already present in normal epidermal cells before tumour formation, we performed FISH analysis using a probe recognizing Chr11 in cytospin of adult basal epidermal cells isolated from control, p53cKO, PLK4OE and PLK4OE/p53cKO adult mice. Remarkably we found that adult PLK4OE/p53cKO epidermal cells contained a higher percentage of cells showing more than 4 dots for Chr11, when compared with control or PLK4OE epidermal cells ($P = 8.886 \times 10^{-10}$ and $P = 1.763 \times 10^{-10}$ respectively; Fig. 6i,j). These findings suggest that certain chromosomal alterations found in PLK4OE/p53cKO tumours were already present in normal epidermal cells before tumour appearance.

These data indicate that the aneuploidy resulting from the transient presence of centrosome amplification during embryonic development persists until adulthood and is responsible for skin tumour initiation. These results also demonstrate that PLK4OE-mediated aneuploidy could be the driving force of skin tumour formation when occurring in a p53-deficient background.

DISCUSSION

Although Boveri suggested that aneuploidy is the cause of cancer more than a century ago[5,8], it remains a matter of long-standing debate whether aneuploidy is the cause or the consequence of tumour formation[9,15]. Our study demonstrates that PLK4OE-mediated centrosome amplification in the presence of p53 is highly deleterious for cell fitness and epidermal development, inducing skin barrier defects and neonatal lethality as previously reported for mice deficient of mitotic kinase aurora A (ref. 11). However, we found that PLK4OE in a p53-deficient background can lead to the survival of some aneuploid cells, which become the precursors of skin tumours, and eventually act as a driver of skin tumorigenesis (Fig. 7).

PLK4OE demonstrates that in the postnatal epidermis very powerful safeguard mechanisms are present to eliminate cells with extra centrosomes by apoptosis. Within a week after birth mCherry–PLK4-expressing cells were no longer detected in the epidermis. These cells were replaced by cells that initially recombined the PLK4 transgene but in which the transgene has been epigenetically/transcriptionally turned off. All PLK4OE cells that contain multiple centrosomes and present multipolar division are eventually eliminated during embryonic development and early postnatal life, demonstrating that PLK4OE-mediated centrosome amplification is incompatible with homeostasis of epidermal cells (Fig. 7). Interestingly and in sharp contrast with the developing mammalian brain[21], deletion of *p53*, although slightly decreasing cell death, did not prevent apoptosis of cells with multiple centrosomes. Further work will be required to identify the exact mechanisms that mediate p53-independent cell death and eliminate epidermal progenitors with an abnormal number of centrosomes and whether other mechanisms besides centrosome duplication may contribute to the phenotypes mediated by PLK4OE.

Although *p53* deletion cannot prevent the eventual elimination of cells expressing more than 2 centrosomes, loss of p53 in PLK4OE cells nevertheless decreases the amount of apoptosis that occurred during embryonic development and neonatally. In addition, p53 loss of function also allows the survival and proliferation of cells with abnormal chromosome content induced by PLK4OE, as previously shown *in vitro*[38]. The few cells that present aneuploidy in PLK4OE/p53cKO epidermis and escape apoptosis during the neonatal period can give rise to skin tumour formation that appeared with a much shorter latency compared with p53cKO tumours (Fig. 7). These data demonstrate that aneuploidy can promote tumorigenesis in the skin epidermis, but only when centrosome amplification is initiated in p53-deficient cells. The high prevalence of *p53* mutations after sunburn[39] and in preneoplastic skin lesions[40], as well as in invasive SCCs (ref. 41), shows that p53 mutation is one of the early genetic events that occurs during skin tumorigenesis and this suggests that transient centrosome amplification may act as a driver of tumorigenesis in this genomic context. Further experiments will be required to assess whether other models inducing centrosome amplification accelerate skin tumorigenesis in p53-deficient epidermis, and whether chronic centrosome amplification is a permissive condition for tumorigenesis as well or instead leads to the complete elimination of cells with extra centrosomes. □

METHODS

Methods and any associated references are available in the online version of the paper.

Note: Supplementary Information is available in the online version of the paper

ACKNOWLEDGEMENTS

C.B. is an investigator of WELBIO; Ö.S. is supported by a TELEVIE fellowship. This work was supported by the FNRS, TELEVIE, the PAI programme, a research grant from the Fondation contre le Cancer, the ULB Fondation, the foundation Bettencourt Schueller, the foundation Baillet Latour, a grant from the European Research Council (ERC) and a grant from AICR now worldwide cancer research (13-0170) to V.M. and R.B.

AUTHOR CONTRIBUTIONS

Ö.S. and C.B. designed the experiments and performed data analysis; Ö.S. performed most of the experiments, J.-C.L. and A.E.K. conducted proliferation experiments; V.M. performed RNA purification; M.L.M. performed FISH experiments; D.L. and B.B. performed tumour sequencing and analysis. V.Ma. and R.B. generated the PLK4OE mice; Ö.S. and C.B. wrote the manuscript.

COMPETING FINANCIAL INTERESTS

The authors declare no competing financial interests.

Published online at http://dx.doi.org/10.1038/ncb3270
Reprints and permissions information is available online at www.nature.com/reprints

1. Nigg, E. A. & Raff, J. W. Centrioles, centrosomes, and cilia in health and disease. *Cell* **139,** 663–678 (2009).

2. Bettencourt-Dias, M., Hildebrandt, F., Pellman, D., Woods, G. & Godinho, S. A. Centrosomes and cilia in human disease. *Trends Genet.* **27,** 307–315 (2011).
3. Firat-Karalar, E. N. & Stearns, T. The centriole duplication cycle. *Phil. Trans. R. Soc.* **369,** 20130460 (2014).
4. Anderhub, S. J., Kramer, A. & Maier, B. Centrosome amplification in tumorigenesis. *Cancer Lett.* **322,** 8–17 (2012).
5. Boveri, T. Concerning the origin of malignant tumours by Theodor Boveri. Translated and annotated by Henry Harris. *J. Cell Sci.* **121,** 1–84 (2008).
6. Lingle, W. L. *et al.* Centrosome amplification drives chromosomal instability in breast tumor development. *Proc. Natl Acad. Sci. USA* **99,** 1978–1983 (2002).
7. Pihan, G. A., Wallace, J., Zhou, Y. & Doxsey, S. J. Centrosome abnormalities and chromosome instability occur together in pre-invasive carcinomas. *Cancer Res.* **63,** 1398–1404 (2003).
8. Holland, A. J. & Cleveland, D. W. Boveri revisited: chromosomal instability, aneuploidy and tumorigenesis. *Nat. Rev. Mol. Cell Biol.* **10,** 478–487 (2009).
9. Weaver, B. A. & Cleveland, D. W. Does aneuploidy cause cancer? *Curr. Opin. Cell Biol.* **18,** 658–667 (2006).
10. Foijer, F. *et al.* Spindle checkpoint deficiency is tolerated by murine epidermal cells but not hair follicle stem cells. *Proc. Natl Acad. Sci. USA* **110,** 2928–2933 (2013).
11. Torchia, E. C., Zhang, L., Huebner, A. J., Sen, S. & Roop, D. R. Aurora kinase-A deficiency during skin development impairs cell division and stratification. *J. Invest. Dermatol.* **133,** 78–86 (2013).
12. Solomon, D. A. *et al.* Mutational inactivation of STAG2 causes aneuploidy in human cancer. *Science* **333,** 1039–1043 (2011).
13. Ricke, R. M., Jeganathan, K. B. & van Deursen, J. M. Bub1 overexpression induces aneuploidy and tumor formation through Aurora B kinase hyperactivation. *J. Cell Biol.* **193,** 1049–1064 (2011).
14. Rao, C. V. *et al.* Colonic tumorigenesis in BubR1+/-ApcMin/+ compound mutant mice is linked to premature separation of sister chromatids and enhanced genomic instability. *Proc. Natl Acad. Sci. USA* **102,** 4365–4370 (2005).
15. Weaver, B. A., Silk, A. D., Montagna, C., Verdier-Pinard, P. & Cleveland, D. W. Aneuploidy acts both oncogenically and as a tumor suppressor. *Cancer Cell* **11,** 25–36 (2007).
16. Chesnokova, V., Kovacs, K., Castro, A. V., Zonis, S. & Melmed, S. Pituitary hypoplasia in Pttg-/- mice is protective for Rb+/- pituitary tumorigenesis. *Mol. Endocrinol.* **19,** 2371–2379 (2005).
17. Sussan, T. E., Yang, A., Li, F., Ostrowski, M. C. & Reeves, R. H. Trisomy represses Apc(Min)-mediated tumours in mouse models of Down's syndrome. *Nature* **451,** 73–75 (2008).
18. Zyss, D. & Gergely, F. Centrosome function in cancer: guilty or innocent? *Trends Cell Biol.* **19,** 334–346 (2009).
19. Basto, R. *et al.* Centrosome amplification can initiate tumorigenesis in flies. *Cell* **133,** 1032–1042 (2008).
20. Sabino, D. *et al.* Moesin is a major regulator of centrosome behavior in epithelial cells with extra centrosomes. *Curr. Biol.* **25,** 879–889 (2015).
21. Marthiens, V. *et al.* Centrosome amplification causes microcephaly. *Nat. Cell Biol.* **15,** 731–740 (2013).
22. Perez-Losada, J. & Balmain, A. Stem-cell hierarchy in skin cancer. *Nat. Rev. Cancer* **3,** 434–443 (2003).
23. Boukamp, P. Non-melanoma skin cancer: what drives tumor development and progression? *Carcinogenesis* **26,** 1657–1667 (2005).
24. Nassar, D., Latil, M., Boeckx, B., Lambrechts, D. & Blanpain, C. Genomic landscape of carcinogen and genetically-induced mouse skin squamous cell carcinoma. *Nat. Med.* **8,** 946–954 (2015).
25. McGranahan, N., Burrell, R. A., Endesfelder, D., Novelli, M. R. & Swanton, C. Cancer chromosomal instability: therapeutic and diagnostic challenges. *EMBO Rep.* **13,** 528–538 (2012).
26. Vasioukhin, V., Degenstein, L., Wise, B. & Fuchs, E. The magical touch: genome targeting in epidermal stem cells induced by tamoxifen application to mouse skin. *Proc. Natl Acad. Sci. USA* **96,** 8551–8556 (1999).
27. Sotiropoulou, P. A. & Blanpain, C. Development and homeostasis of the skin epidermis. *Cold Spring Harb. Perspect. Biol.* **4,** a008383 (2012).
28. Kleylein-Sohn, J. *et al.* Plk4-induced centriole biogenesis in human cells. *Dev. Cell* **13,** 190–202 (2007).
29. Holland, A. J. *et al.* The autoregulated instability of Polo-like kinase 4 limits centrosome duplication to once per cell cycle. *Genes Dev.* **26,** 2684–2689 (2012).
30. Blanpain, C., Lowry, W. E., Pasolli, H. A. & Fuchs, E. Canonical notch signaling functions as a commitment switch in the epidermal lineage. *Genes Dev.* **20,** 3022–3035 (2006).
31. Koster, M. I. & Roop, D. R. Mechanisms regulating epithelial stratification. *Annu. Rev. Cell Dev. Biol.* **23,** 93–113 (2007).
32. Sancar, A., Lindsey-Boltz, L. A., Unsal-Kacmaz, K. & Linn, S. Molecular mechanisms of mammalian DNA repair and the DNA damage checkpoints. *Annu. Rev. Biochem.* **73,** 39–85 (2004).
33. Sotiropoulou, P. A. *et al.* Bcl-2 and accelerated DNA repair mediates resistance of hair follicle bulge stem cells to DNA-damage-induced cell death. *Nat. Cell Biol.* **12,** 572–582 (2010).
34. Lechler, T. & Fuchs, E. Asymmetric cell divisions promote stratification and differentiation of mammalian skin. *Nature* **437,** 275–280 (2005).
35. Williams, S. E., Ratliff, L. A., Postiglione, M. P., Knoblich, J. A. & Fuchs, E. Par3-mInsc and Galphai3 cooperate to promote oriented epidermal cell divisions through LGN. *Nat. Cell Biol.* **16,** 758–769 (2014).
36. Izumi, H. & Kaneko, Y. Evidence of asymmetric cell division and centrosome inheritance in human neuroblastoma cells. *Proc. Natl Acad. Sci. USA* **109,** 18048–18053 (2012).
37. Liu, X. *et al.* Somatic loss of BRCA1 and p53 in mice induces mammary tumors with features of human BRCA1-mutated basal-like breast cancer. *Proc. Natl Acad. Sci. USA* **104,** 12111–12116 (2007).
38. Holland, A. J., Lan, W., Niessen, S., Hoover, H. & Cleveland, D. W. Polo-like kinase 4 kinase activity limits centrosome overduplication by autoregulating its own stability. *J. Cell Biol.* **188,** 191–198 (2010).
39. Ziegler, A. *et al.* Sunburn and p53 in the onset of skin cancer. *Nature* **372,** 773–776 (1994).
40. Berg, R. J. *et al.* Early p53 alterations in mouse skin carcinogenesis by UVB radiation: immunohistochemical detection of mutant p53 protein in clusters of preneoplastic epidermal cells. *Proc. Natl Acad. Sci. USA* **93,** 274–278 (1996).
41. Ruggeri, B. *et al.* Alterations of the p53 tumor suppressor gene during mouse skin tumor progression. *Cancer Res.* **51,** 6615–6621 (1991).

METHODS

Mice. The *mCherry–Plk4* transgenic mouse strain (generated from the C57Bl6/N strain) was obtained from R. Basto (Centre de Recherche , Institute Curie, Paris, France)[21]. *K14CRE* mice (generated from CD-1 strain) were a gift from E. Fuchs[26] (Howard Hughes Medical Institute, The Rockefeller University, New York, USA). $p53^{fl/fl}$ (FVB/N strain) mice were obtained from the National Cancer Institute at Frederick[42]. *K14CRE* mice were mated with *PLK4* and $p53^{fl/fl}$ mice. All experimental mice were therefore from a mixed background. Mouse colonies were maintained in a certified animal facility in accordance with European guidelines. No statistical method was used to predetermine sample size. The experiments were not randomized and the investigators were not blinded to allocation during experiments and outcome assessment. Embryos, pups and adults from both genders were analysed randomly. The observation of a vaginal plug was considered as day 0.5 of embryonic development. Mice were genotyped from their tail and or fingers.

Toluidine dye penetration assay. We performed the assay as described previously[11]. E17.5 embryos were dehydrated through a gradient of methanol 25%, 50%, 75% and 100% for 30 s each, respectively; and then rehydrated 100% to 25% methanol and finally incubated in PBS for 3 min. All embryos were stained in 0.1% toluidine (Sigma Aldrich) for 10 min and then washed for 30 min in PBS.

Macroscopic pictures. Pictures were taken after toluidine dye assay under direct sunlight using a D70 Nikon camera (Nikon).

Histology, immunostaining, cell extraction and imaging. Tissues from mice were processed in OCT (Sakura) and sections were fixed in 4% PFA for 10 min at room temperature. Samples were cut into 5–8 µm sections using a CM3050S Leica cryostat (Leica Microsystems GmbH). For haematoxylin–eosin and p53 stainings paraffin blocks of tissues prefixed overnight in 4% PFA were sectioned using an HM560 Microm microtome (Mikron Instruments) into 5 µm sections.

The following primary antibodies were used for OCT sections: anti-K14 (chicken, 1:2,000, Covance, SIG-3476-0100), anti-β4 (rat, 1:200, BD, 346-11A), anti-K1 (rabbit, 1:2,000, Covance, PRB-165P-0100), anti-K10 (rabbit, 1:2,000, Covance, PRB-159P-0100), anti-K8 (rat, 1:500, Troma, DSHB), anti-vimentin (rabbit, 1:200, Abcam, EPR3776), anti-NuMA (rabbit, 1:1,000, Novus Biologicals, NB500-174), anti-active-caspase 3 (rabbit, 1:1,000, R&D, AF835), anti-loricrin (rabbit, 1:1,000; Covance, PRB-145P-0100), anti-EpCam (rat, 1:500, BD, 563134), anti-Ecad (rat, 1:500, eBioscience, 14-3249-82). Sections were incubated in blocking buffer (horse serum 5%, BSA 1%, Triton 0.2% in PBS) for 1 h at room temperature. Primary antibodies were incubated overnight in the same blocking buffer at 4 °C. Sections were rinsed three times in PBS and incubated with secondary antibodies diluted at 1:500 in blocking buffer for 1.5 h at room temperature. The following secondary antibodies were used: anti-rabbit and anti-rat conjugated to AlexaFluor488 (Molecular Probes) or to rhodamine red-X or Cy-5 (Jackson Immuno Research) with respect to the antibody that was used as the primary. Nuclei were stained in Hoechst solution (1:4,000) and slides were mounted in DAKO mounting medium supplemented with 2.5% Dabco (Sigma).

Immunohistochemistry of p53 was performed as previously described[43]. Sections were processed for deparaffinization. Slides were then processed for antigen retrieval for 20 min at 98° C in citrate buffer (pH 6) (ScyTek) using the PT module (Lab Vision). To inhibit endogenous peroxidase we used 3% H_2O_2 (Merck) in methanol for 10 min at room temperature. Following 3 consecutive PBS washes to remove methanol, to block endogenous avidin and biotin, we used the Endogenous Blocking Kit (Invitrogen) for 20 min at room temperature. Slides were then blocked with M.O.M. Blocking kit with 0.2% Triton X-100 (Sigma for 1 h). Following a single PBS wash, mouse anti-p53 antibody (clone 1C12; Cell Signaling) was incubated overnight at 4 °C. After 3 PBS washes, we used biotinylated anti-mouse in M.O.M. Blocking kit for 1 h at room temperature, washed 3 times with TBS-T (20 mM Tris pH 7.6, 100 mM NaCl, 0.2% Tween-20 (Sigma)) and then we used the protocol from Vector Laboratories for the Standard ABC kit, and the ImmPACT DAB to reveal HRP signal for 3 min and 30 s. Signal was quenched by washing in tap water and slides were then dehydrated using an ethanol gradient followed by Safe Solvent and mounted using SafeMount (Labonord).

For keratinocyte extraction we used the following protocol. Embryos or newborns were euthanized and skin was removed and placed on 1% Dispase (Sigma) in HBSS (Gibco) and incubated overnight. The following day, the epidermis was carefully separated from the dermis using forceps and placed on 0.25% trypsin with 1 mM EDTA in DMEM (Gibco) for 15 min at 37°. The tissue was slowly dissociated into single cells by pipetting and trypsin was neutralized by addition of 5% CFCS (chelated fetal calf serum) in DMEM. This suspension was then passed through a 40 µm (BD) filter to remove debris and allow a single-cell suspension. After 5 min 250*g* centrifugation, cells were resuspended in PBS and 50,000 cells were cytospun on slides for cytospin (Cellspin Tharmac) by centrifugation at 300 r.p.m. for 3 min.

For tubulin staining, dissociated cells on slides prepared with cytospin were fixed in methanol (prechilled −20 °C) for 15 min and washed with PBS and stored at 4 °C until stained. Samples were blocked with 1% BSA for 1 h and stained with the same buffer using antibodies at the following concentrations: anti-K14 (chicken, 1:3,000, Covance), anti-PH3 (rat, 1:3,000, Abcam HTA28), anti-γ-tubulin (rabbit, 1:2,000, Sigma T5192), anti-α-tubulin (mouse, 1:2,000, Sigma DM1A) for 1.5 h at 37 °C. Samples were washed with PBS 3 times and incubated with secondary antibodies coupled to AlexaFluor488 (Molecular Probes), rhodamine red-X or Cy-5 (Jackson Immuno Research) in PBS with 1% BSA for 1 h. Samples were mounted with DAKO mounting medium supplemented with 2.5% Dabco (Sigma).

For FISH analysis, cytospin samples were fixed with 4% PFA and washed with PBS and stored at 4 °C until stained. Slides were quickly rinsed by immersing into distilled water to remove PBS. Slides were then dried and then baked at 56 °C for 2 h and rehydrated in an ethanol gradient 100%, 85% and 70% for 1 min each and finally in distilled water for 3 min at room temperature. We followed solutions and protocols from Kreatech (KBI-60007 kit) and the Zytovision FISH cytology kit (Z-2099-20). The probes were obtained from ID-Labs (Empire Genomics) for mouse Chr16 (D16Mit88) and Chr15 (D15Mit224) and Chr11 (D11Mit188).

Pictures were acquired using the Axio Imager M1 microscope, the AxioCamMR3 or MrC5 camera and using the Axiovision software (Carl Zeiss). The measurements for skin thickness were performed with Axiovision software tools. The numbers of centrosomes were counted in intact nuclei in at least 3 mice for each group and the number of cells is denoted in the figure legends. The number of tumours per mouse and the number of mice that developed tumours were entered into the Prism survival curve function and graphs were generated using GraphPad Prism and *t*-tests were also carried out by Prism software.

Cell sorting. Tumours from PLK4OE/p53cKO mice were digested with collagenase following a protocol as previously described[24]. Single-cell suspensions were stained for markers: CD31 (PE, rat, 1:200, BD 12-0311), CD140a (PE, rat, 1:200, eBioscience, 12-1401/624049), CD45 (PE, rat, 1:200, eBioscience 12-0451/553081) and Hoechst and gates were selected to exclude debris, dead cells and non-epidermal cells.

Genomic DNA extraction. Genomic DNA was extracted from FACS-isolated cells or bone marrow cells using the Qiagen DNeasy Blood & Tissue kit following the manufacturer's instructions.

PCR analysis for recombination of PLK4 transgene. Forward (5′-GCAACG TGCTGGTTATTGTG-3′) and reverse (5′-AAGCGCATGAACTCCTTGAT-3′) recombination specific primers that surround both *loxP* sites (if not recombined) or one *loxP* site (if recombined) were designed as demonstrated in Supplementary Fig. 1b and used with 100 ng of genomic DNA at 40 cycles with the following programme: 60 °C annealing for 15 s and 72 °C extension for 25 s using SyBr I Green Master Mix (Roche). Both recombined and non-recombined bands were cut from the agarose gel, extracted and sequenced with the same primers to confirm recombination.

qPCR analysis for recombination of PLK transgene. Forward (5′-GAGCTT GGCGAGATTTTCAG-3′) and reverse (5′-AAGCGCATGAACTCCTTGAT-3′) specific primers that amplify only the unrecombined allele were designed as shown in Supplementary Fig. 1a and forward (5′-TGGCTGGCCGGGACCTGA-3′) and reverse (5′-ACCGCTCGTTGCCAATAGTGATGA-3′) primers were used to amplify the housekeeping gene, β-actin. PCR was performed using 100 ng of genomic DNA during 40 cycles with the following cycle: 60 °C annealing for 15 s and 72 °C extension for 150 s using SyBr I Green Master Mix (Roche) and Roche LP96 using the manufacturer's instructions.

qRT–PCR analysis of mCherry–PLK4 expression. Total RNA from skin epidermis was extracted using the Qiagen RNeasy MicroKit using the manufacturer's instructions. Reverse transcription was performed using Random Hexamers (Roche) and using Invitrogen SuperScript II Reverse Transcriptase and using the manufacturer's instructions.

Forward (5′-GCGTGATGAACTTCGAGGA-3′) and reverse (5′-TTGACCTCA GCGTCGTAGTG-3′) specific primers for mCherry with 8 ng of cDNA at 40 cycles with the following programme: 60 °C annealing for 15 s and 72 °C extension for 20 s using SyBr I Green Master Mix (Roche) and Roche LP96 using the manufacturer's instructions. Fold change was calculated using the ΔΔCT method and using β-actin as a housekeeping gene. If CT was undetected, it was considered as 40 cycles to enter quantification.

Low-coverage whole-genome sequencing. Data related to Fig. 6k are available from ArrayExpress E-MTAB-3733.

DOI: 10.1038/ncb3270

42. Jonkers, J. *et al.* Synergistic tumor suppressor activity of BRCA2 and p53 in a conditional mouse model for breast cancer. *Nat. Genet.* **29,** 418–425 (2001).

43. Sotiropoulou, P. A. *et al.* BRCA1 deficiency in skin epidermis leads to selective loss of hair follicle stem cells and their progeny. *Genes Dev.* **27,** 39–51 (2013).